Evaluation of shallow cycling on uncompressed $Li(Ni_{1/3}Mn_{1/3}Co_{1/3})O_2$-Graphite pouch cells with 40 and 44 Ah

Authors

Meinert Lewerenz[a], Christiane Rahe[b,c], Georg Fuchs[c,d], Christian Endisch[a] and Dirk Uwe Sauer[b,c,d]

Affiliation

a) Research Group Electromobility and Learning Systems, Technische Hochschule Ingolstadt, D-85049, Germany

b) Helmholtz Institute Münster (HI MS), IEK-12, Forschungszentrum Jülich, Jägerstraße 17-19, 52066 Aachen, Germany

c) Juelich Aachen Research Alliance, JARA-Energy, Germany

d) Electrochemical Energy Conversion and Storage Systems Group, Institute for Power Electronics and Electrical Drives (ISEA), RWTH Aachen University, Jägerstrasse 17/19, D-52066 Aachen, Germany

Abstract

For this contribution, two generations of uncompressed pouch cells are investigated in cyclic aging tests. The results are evaluated opposing both cell generation and highlighting the differences to compressed cells reported in literature. The cells are evaluated with respect to pulse resistance, anode overhang, dV/dQ-analysis, capacity difference analysis, homogeneity of lithium distribution (HLD) and irreversible capacity losses. It is shown, that uncompressed

cells reveal, in contrast to compressed cells, a higher HLD, which is demonstrated in the missing dV/dQ flattening over aging. The trends of peak heights in dV/dQ depends mainly on the graphite voltage and expansion characteristics and is therefore different for both cell generations due to different degree of utilization of the anode. The trends are comparable to calendric aging test results. The irreversible losses for uncompressed cycled cells increase with cell potential while compressed cells show higher losses to lower and higher SOCs caused by low HLD. Thus, in compressed cells there is a higher risk for lithium plating for inhomogeneous distributed active lithium in accelerated aging tests. Comparing both cell generations, the lifetimes show strong deviations and the largest impact is associated to n/p ratio of the anode to the cathode.

Key Words

Pressure; dilation; cyclic aging; differential voltage analysis; irreversible capacity loss; Uncompressed; pouch

Abbreviations

FCE: full cycle equivalents

DVA: differential voltage analysis

PMA: Post-mortem-analysis

DOD: depth-of-discharge

SOC: state-of-charge

1. Introduction

Today, rechargeable lithium-ion cells are used in a wide spectrum from mobile to stationary applications. The cell housing varies from pouch bag, over cylindrical to prismatic. The housing influences the utilization of space in a battery pack but they also lead to a different compression of the jelly roll or the stack.

There are several publications dealing with volume work of cells. The volume change arises on one hand from contraction and expansion in the order of 12% [1] of mainly the graphite anode during cycling [2]–[4] and on the other hand from swelling that occurs during aging [5]–[7].

The volume expansion leads to pressure on the jelly roll/stack, in case the housing limits the expansion or the cell is externally compressed [8]. In some publication certain pressure is regarded to have positive influence on cell performance [3],[8]–[10] and in others, to have negative influence [11], especially applying very high pressure [12]. In case of inhomogeneously distributed pressure on the electrode, lithium metal deposition occurs very likely due to local overcharge [13]–[16]. To understand the difference of the presence and absence of pressure, a short excursus with respect to the impact of compression on cells is given in the following.

Pressure on the stack or jelly roll compresses the active materials and the usually soft polyolefin separator [12]. Both current collectors are not considered to be compressible under reasonable pressure (<1 MPa [1]). The coated active materials are nowadays calendered with very high pressure of 10 to 30 MPa (100-300 kg/cm³) [17] to increase the volumetric energy density [18] resulting in porosities in the range of 10-40%. It is very unlikely that reasonable external compressions of 222-742 kPa [3] will destroy previously calendered active material particles. Thus, loss of active material is not significantly caused by reasonable external compression. However, loss of active material takes place especially under cycling induced volume change.

Looking closer, the coating is composed not only of active material but as well of a binder / conductive additive composition, which has a certain elasticity. Therefore, pressure leads, on one side, to a decrease of porosity, and on the other side, to a decrease in electrode distance and a more compact electrode with improved electrical contact. Assuming an insufficient adhesion of the coating on the current collector, reasonable pressure guarantees electrical

contact. The separator itself is very porous and very compressible. An increase of external compression will lead on one hand to a lower thickness of the separator but on the other hand to blocked pores. Latter decreases the ionic conductivity between anode and cathode. For e.g. graphite with large spherical particles, it is very likely that pressure will block the separator only locally on the curvature of the outermost particles while the interstitial space remains uncompressed, and with this, the separator remains mainly unblocked. Under extreme pressure, the separator behaves plastic and the pores close, impeding lithium-ion exchange [19]. To sum up, pressure can lead to a performance improvement, but eventually also to a deterioration depending on the actual cell setup and the properties of the cell components.

Assuming that external pressure improves performance, locally higher pressure leads to faster charging of this electrode area compared to the residual electrode. In [9] it was reported that a locally higher pressure, caused by thick covering layer, combined with full cycles leads to a charge accumulation, and with this, to a self-acceleration of lowering homogeneity of lithium distribution (HLD). HLD is a measure for the distribution of SOC over the electrode. HLD is measured by evaluating characteristic peaks of the graphite anode in differential voltage analysis (DVA) [10]. Sharp peaks, i.e. increased peak heights, are associated with high HLD and a flattening of the peak with a lower HLD. In [10],[20] it was shown that shallow cycling of cells with limited space show higher capacity losses towards lower and higher SOC (u-shape) and in [10],[21] additionally a reduction of HLD was presented. In [22], it was shown that a large portion of capacity and HLD is recoverable by storing the cell for more than 100 days at 20 °C. Thus, this is proof for the reversibility of HLD and the influence of a low HLD on extractable capacity. Epding et al. [23] presented in their work that test pauses in accelerated cycling tests for compressed prismatic cells have a strong impact on aging and during pauses extractable capacity increases. Grandjean et al. [24] observed in a cyclic aging test strong capacity recovery during test pauses for an 18650 cell with limited space while no such recovery is measured for uncompressed pouch cells. They further state that all tested cells are stopped and started at exactly the same time. All these results support the findings presented before. Generally, HLD reduction is directly associated to cycling as no flattening of peaks in DVA is reported for calendric aging [3],[13],[25],[26].

As already mentioned, the compression of the cells is crucial for their performance and cycle life. In order to better understand and evaluate the impact of compression, it is important to know, how a cell without compression is behaving. Käbitz et al. [27] investigated an unconstrained pouch cell with shallow cycling at different average SOCs. The irreversible

capacity loss (neglecting anode overhang effect [3]) increases with average SOC. Unfortunately, the DVA, and with this, HLD were not investigated in this publication.

To best of our knowledge, a focus of the comparison between compressed and uncompressed cells for shallow cycling, including anode overhang effect and homogeneity of lithium distribution (HLD), is missing in literature. In this publication, a theory for uncompressed cells under cyclic aging is given and compared to results of compressed cells reported in literature. Therefore, for different SOCs shallow cyclic aging tests are evaluated for this work for an uncompressed pouch cell in a standard setup (generation 1/ GEN-1) and in an improved cell setup (generation 2/ GEN-2) with lower n/p ratio, less anode overhang and higher energy density. In section 4.1 the extractable capacity and resistance is presented. Thereafter, results are correlated in sections 4.2 and 4.3 with capacity difference analysis (CDA) and the DVA series and peak heights to determine HLD. Finally, in section 4.4 the irreversible aging is assessed by linear regression of the last part of capacity trend and the two cell designs are compared to each other.

2. Experimental

2.1 Electrical characterization

In this contribution, 24 stacked NMC|Graphite lithium-ion pouch cells are investigated in a cyclic aging test. All cells are produced and provided by the German/Canadian manufacturer *Litarion (bankcrupt in 2018)*. The first 12 cells represent the GEN-1 cell (LITACELL LC-40) of Litarion and the last 12 cells are the GEN-2 version (LITACELL LC-44) of the cell. For the GEN-2 version the energy density is increased, the anode overhang is decreased and the anode is utilized at a higher degree (n/p ratio see ANNEX). The voltage (SOC) before test is the voltage the cell was delivered and cannot be defined by the authors. The SOC is measured thereafter in a 1C discharge. The specific information for both cell generations are given in Table 1. Further results of the post-mortem-analysis and preliminary tests according to the cells will be given in section 3.

All tests are conducted at 1C 6% DOD around an average SOC specified in Table 2 on the two left columns. The GEN-1 design is tested at a defined OCV voltage while the GEN-2 cell design is tested at defined SOC with respect to the anode voltage characteristics. Consequently, the test SOC is measured in each check-up and the test SOC is adjusted with aging. However, as the irreversible capacity loss is very low in this cycling test, the deviation of both SOC definitions are therefore negligible. The principle is presented in [3],[10] in-depth.

The dV/dQ curves of a discharge are depicted in Figure 1 a) for the GEN-1 and b) for the GEN-2 cell design. The corresponding average SOC is included in both figures.

The aging tests are interrupted by check-up tests. During a check-up, 1C and 0.1C capacity tests and a pulse test are included. The check-up and aging temperature is 20 °C. For capacity tests, the cells are charged CCCV to 4.2 V until a current of 0.02C is reached. After a 10 min

rest, the cell is discharged in a CC mode down to 3.0 V. The pulse tests are evaluated at 50% SOC at 1C discharge after 10 s. A more detailed description of the check-ups is ruled out in [3].

Table 1 Specifications of the used battery

	GEN-1	**GEN-2**
Type	LITACELL LC-40	LITACELL LC-44
Cathode	NMC, 1:1:1	
Anode	Graphite	
Separator	ceramic	
Charge cut-off voltage	4.2 V	
Discharge cut-off voltage	3.0 V	
Nom. Capacity @ 0.5C	40 Ah	44 Ah
Energy density	152 Wh/kg	162 Wh/kg
Full anode overhang	8.6%	6.1%
Near anode overhang	5.5%	3.3%
Voltage (SOC) before test	3.66 V (40%)	3.64 V (35%)
n/p ratio	1.56	1.39

Table 2 Testmatrix: The cells are cycled around the five named average SOCs / voltages with a C-rate of 1C and a DOD of 6%. In the two right columns, the average SOC with respect to the anode capacity is given resulting from the n/p ratio.

Average SOC (cell)		**Average SOC (Anode)**	
GEN-1	GEN-2	GEN-1	GEN-2
76% (3.88 V)	80%	52%	65%
61% (3.74 V)	68%	41%	56%
41% (3.63 V)	45%	28%	34%
18% (3.51 V)	22%	13%	16%

5% (3.34 V)	10%	8%	8%

2.2 Preliminary characterization

Preliminary tests and characterization are conducted for both cell types. The cells are dismantled in an Ar-filled glovebox. The stoichiometry is investigated using Varian ICP-OES (Inductively Coupled Plasma- Optical Emission Spectrometer). The porosity of the coating is measured with an Hg-porosimeter up to 400 MPa (Thermo Fisher Pascal 140/440). The morphology of the coating is investigated using Keyence VK-9710 lasermicroscope. The layer thickness of the coating was measured with a micrometer screw with an accuracy of +/-1 µm. For electrochemical investigation, punched out discs with 16 mm diameter of anode and cathode are inserted in coin cells vs. lithium metal (half-cells). The half-cells are cycled at C/10. The cell expansion and contraction for both cells are measured by an Extramess 2000 inductive dial comparator of the company Mahr. The resolution is 1 µm and a span of error of 0.6 µm.

3. Preliminary characterization

3.1 Post mortem analysis

The geometries of the cells are given in Figure 2 for GEN-1 (a) and GEN-2 (b) to obtain the anode overhang and the corresponding distances to the active anode. The anode overhang ratio is defined by the coated area of the anode divided by the coated area of the cathode (⇔ active anode area) according to [3]. GEN-2 shows a lower anode overhang by smaller oversize of the anode. In an arbitrary definition, the near part of the anode overhang includes only the oversized anode facing the cathode, while the full anode overhang includes as well the two outer double-coated anode with no opposed cathode (Table 1). The stacking strategy and the parts of the anode overhang are additionally sketched in c). Besides active materials, the energy density is increased from GEN-1 to GEN-2 by smaller anode overhang and lower n/p ratio. The total capacity is further increased by additional three sheets of anode and cathode (Table 1).

The stoichiometry of the cathode of a 1:1:1 NMC is confirmed by ICP measurements for both cell types. The results of porosimeter measurements including additional parameters are summarized in Table 3. The results of the coating morphology of pristine electrodes using lasermicroscope are presented in Figure 3 for a) the anode and c) the cathode of the GEN-1 and for b) the anode and d) the cathode of the GEN-2 cell design. The morphology of anode and cathode for both cell designs is comparable. Only on the anode of GEN-1, some additional smaller particles are detected. The results of the layer thickness of the coating, given in Table 3, support the assumption of a higher n/p ratio of the GEN-1 cell design. While the cathodes have more or less the same thickness, the anode of the GEN-1 cell is significantly thicker.

The discharge curves of half-cells for anode and cathode and their derivatives are given in Figure 4. Comparing the results with full cell characteristics in Figure 1, the minima are clearly attributed to the anode (Figure 4a) while the slope change at high voltages is assigned to the cathode (Figure 4b). For the GEN-2 cell design, the voltage characteristics of the anode are typical for graphite reported in literature [3],[13],[28]. The purity or crystallinity of graphite in the GEN-2 cells seems to be higher than for the GEN-1 cells. Thus, it is likely that in the GEN-1 cells some amorphous fraction of hard carbons might be included [29]. The theory of a composite material is further supported by the fact that the peak at stage 2 appears at more than 50% lithiation [30]. For the cathode the voltage trends fit very well to the standard 1:1:1 [3] as it is supported by ICP-OES results.

Table 3 Porosities, particle diameter, inner surface, skeleton density and layer thickness of the coating of the examined cells

		GEN-1	GEN-2
Anode	porosity	23%	23%
	avg. diameter	0.2 µm	0.6 µm
	Inner surface	2.2 m^2/g	0.7 m^2/g
	Skeleton density	1.98 g/cm^3	2.00 g/cm^3
	Layer thickness	66 µm	58 µm
Cathode	porosity	24%	20%
	avg. diameter	0.5 µm	1 µm
	Inner surface	1.1 m^2/g	0.5 m^2/g
	Skeleton density	2.90 g/cm^3	2.83 g/cm^3
	Layer thickness	57 µm	56 µm

3.2 Volume work of the cell

The displacement for a discharge is shown in Figure 5a for two measurement positions (solid: position 1, dashed: position 2). For both cell types, a strong increase of 120 µm and 150 µm is measured at low SOC, followed by an only slightly increasing part. In the last part the slope of displacement increases again. This is mainly assigned to the expansion characteristics of the graphite anode. Especially the last part of the slope increase appears to be very small and less pronounced for the GEN-1 cell design. This is another indicator for a lower crystallinity of the graphite and additional amorphous hard carbons. For the GEN-1 cell design, the expansion is less pronounced with 175 µm compared to the GEN-2 cell design with 250 µm. This matches to the peak characteristics of the full cell DVA attributed to the anode in Figure 5b and the higher n/p ratio of the GEN-1 cell design.

4. Results and discussion

The test results are presented for the two types of uncompressed cells. In section 4.1 the capacity and resistance trends are given and the share of anode overhang on the extractable capacity is outlined. In sections 4.2 and 4.3, the trend of homogeneity of lithium distribution and their influence on extractable capacity is discussed. Finally, the irreversible losses excluding reversible effects are focused in section 4.4.

The tests results are compared on one side to results reported for compressed cells in literature and on the other side both optimization strategies (GEN-1 and GEN-2) are opposed to each other.

4.1 Capacity and resistance trends over aging

The capacity tests and the internal resistance for the GEN-1 and the GEN-2 cell design are presented in Figure 6.

The results of the capacity tests Figure 6a and b show for both cells an increase of extractable capacity loss with increasing test SOC. At significantly lower SOCs compared to the delivery SOC (GEN-1: 40% / GEN-2: 35%), the extractable capacity rises above 100%. For significantly higher SOCs compared to the delivery SOC, the extractable capacity shows an initial drop within the first 500 FCE. At around 40% SOC (blue curves) the linear extrapolation of the trend to 0 FCE is close to 100% capacity. This is the case for the GEN-1 as well as for the GEN-2 cell design.

The internal resistance in Figure 6c and d exhibits for both cells only a small increase of less than 20% over aging. Considering both cell designs, no correlation of internal resistance to the test SOC is observable. For clarification, in Figure 6c at 1200 FCE and in Figure 6d at 1500 FCE the resistance measurement is clearly erroneous as they showed extreme low values that do not follow the overall trend and are therefore deleted from the graph.

Qualitatively, the results for the capacity trend are in line with the theory about the anode overhang [3],[31],[32]. In case the SOC during test is higher than the delivery SOC, lithium-ions move from the active anode to the anode overhang. Within the 10 h discharge, the lithium-ions in the anode overhang are not available anymore as path length for the lithium-ions increases from µm between active anode and cathode to mm or cm range between anode overhang and cathode. In case the test SOC and the delivery SOC are equal, no lithium-ion flow from or to the anode overhang is triggered. Is the average test SOC lower than the delivery SOC, lithium-ions move from the anode overhang to the active anode. In that case, the active lithium from the anode overhang becomes cycable within the 10 h discharge and the extractable capacity rises beyond 100% with respect to the initial capacity. Thus, the behavior of the capacity trend within the first 500 FCE is dominated by the influence of the anode overhang, as it was reported before for cylindrical [31], pouch [33] and prismatic cells [3],[10].

As presented before, the anode overhang is separated by arbitrary definition in a near part of the anode overhang and the full anode overhang including the far part (see experimental). The near part is represented by the oversized sheets in the order of mm to the active anode. The full anode overhang includes additionally the back side of the very outer anode sheets and has a distance of cm to the active part. The theoretical calculated lithium-ions moved to the anode overhang for the near and the full anode overhang are given in Table 4 and Table 5. They are calculated according to [3]:

$$\Delta C_{test}^{calc} = (\mathrm{SOC}_{t=0} - \mathrm{SOC}_{\mathrm{test}}) \cdot \left(\frac{A_{Anode}}{A_{Cathode}} - 100\%\right) \quad (1)$$

Under the assumption that the regular aging is near-linear, the extrapolation to the y-axis exhibits the share of lithium-ions that is moved from or to the anode overhang (graphical method) [3]. In Table 4 and Table 5, the results are given for the GEN-1 and the GEN-2 cell design. For both cell types, the correlation with the near part of the anode overhang is best.

Consequently, one can conclude that the far part contributes hardly to the lithium-ion movement or has extreme long time constants. This is in line with the findings of Warnecke [34] who showed optically for a 20 Ah pouch cell that only a frame of 2 cm of the outer anode sheets is fully lithiated while the residual parts are only partly lithiated (ICP measurement). This implies that a smaller fraction of the anode overhang in equation (1) is fully usable in a reasonable test time.

The comparison of the theoretical calculated near part of the anode overhang and the graphical obtained lithium-ion movement are shown in Figure 7 as a function of the test SOC. Considering the blue curve, a linear relationship is observable and the values for both cell types are in the same order. As both cell types have a different anode overhang size but nearly the same interface, considering active anode and anode overhang, the size of the anode overhang seems to have less influence compared to the interface. Thus, it is assumed that a part of the near anode overhang is cycled during a discharge and does not appear as an overhang but as active anode.

Table 4 Comparison of the expected lithium-ion movement from and to the anode overhang for the GEN-1 cell design.

Test SOC	Measured movement	Expected near Anode ovg	Expected full Anode ovg	Lasermicroscope identified ratio of Anode overhang
76%	-0,5%	-2,0%	-3,1%	-0,5%
61%	-0,3%	-1,2%	-1,8%	-0,3%
41%	0,2%	-0,1%	-0,1%	0,0%
18%	0,7%	1,2%	1,9%	0,3%
5%	0,9%	1,9%	3,0%	0,5%

Additionally, the lasermicroscope images are evaluated to determine the used anode overhang. Comparing the photographs and lasermicroscope images of the far anode overhang

of a pristine (formatted) cell with aged cells, one observes that the aged cells especially on the anode overhang are covered with a dense µm-thick covering layer. Due to the ICP-OES measurements, the lithium concentration on the far anode overhang is lowest in the center part while a frame closer to the active part reveals higher concentrations. The covering layer consist according to ICP of electrolyte components while no higher content of Mn is measurable. Agubra et al. [35] wrote already, that EC out of the electrolyte is highly reactive and results in a growing anode surface layer. Smith et al. [36] discovered, that cells cycled at lower rates have a larger capacity loss than cells cycled at higher rates. Another reason could be that during formation no defined conditions in the anode overhang part are achieved as it is the case for the active anode, which would result in a worse quality of the SEI after formation in the anode overhang area.

The presence of covering layer increases the internal resistance by additional barriers of the covering layer and by less available electrolyte. The covering layer further will impede Li-ion exchange in certain crystallites, so that active material is partly deactivated. Therefore, only a part of the anode overhang is actively usable.

Table 5 Comparison of the expected lithium-ion movement from and to the anode overhang for the GEN-2 cell design.

Test SOC	Measured movement	Expected near Anode ovg	Expected full Anode ovg	Lasermicroscope identified ratio of Anode overhang
80%	-0,6%	-1,5%	-2,7%	-0,9%
68%	-0,3%	-1,1%	-2,0%	-0,7%
45%	0,0%	-0,3%	-0,6%	-0,2%
22%	0,4%	0,4%	0,8%	0,3%
10%	0,6%	0,8%	1,5%	0,5%

For a quantitative analysis, the ratio of the covered area of the overhang was determined for the 5% SOC cell for GEN-1 and 80% SOC cell for GEN-2 exemplarily. If just the areas without a cover layer are taken into account for the usable overhang calculation, the overhang is estimated to about 1.5%±0.3% for GEN-1 (see Table 4) and to about 2%±0.3% for GEN-2 (see Table 5). This optically determined usable anode overhang fits better to the Li-ion movement measured with linear extrapolation (graphical method).

This is further supported by the findings evaluating the capacity differences in the following section.

4.2 Capacity difference analysis

For the capacity difference analysis (CDA) the difference of the discharge capacities measured at 1C and at 0.1C is evaluated. The results are shown in Figure 9a for the GEN-1 and in Figure 9b for the GEN-2 cell design. Contrary to findings in [3],[10],[37], the capacity difference remains constant or even rises within the first 1000 FCE. Only for SOCs higher than 60%, the capacity difference shows a slow decline. Despite, the results of the calendric aging tests, shown in an upcoming publication, lead to a decline of capacity difference for all cells. Finally, all cells in all test conditions reach the corridor sketched with a grey bar in Figure 9.

The results of capacity difference of a compressed prismatic cell during cyclic aging tests give a different picture [10]. They show a reduction and intend to reach the grey part after about 500 FCE under comparable aging conditions and with a comparable cathode stoichiometry. However, up to 400 FCE the capacity difference starts rising or settles at a lower value. Thus, the pressure seems to have a lucid influence as in [37] comparable observations are reported for a cylindrical cell. In [37], the decline was associated to the successively deteriorated lateral transport of lithium ions from and to the anode overhang. Following this theory, the lateral transport for the examined unconstrained pouch cell is not affected. This would match

to the findings, considering the unexpectedly low relative lithium-ion movement values, dedicated to the anode overhang.

As the capacity difference of the cells in Figure 9 are not continuously rising, this is an indicator for a high homogeneity of lithium distribution (HLD). The HLD is further discussed in the following section.

4.3 Differential voltage analysis (DVA)

The DVA is shown in Figure 10 for the GEN-1 and in Figure 11 for the GEN-2 cell. In each diagram, the DVA series over the aging are plotted for each check-up at a specific average SOC. The color of the curves is linked to the capacity fade according to a linear interpolation excluding the anode overhang effect (see section 4.4). For all average SOCs and for the GEN-1 and the GEN-2 cell design, the shape of the DVA is not significantly changing over aging. The slight shape change is visible only in Figure 11a) from the 2^{nd} to the 5^{th} check-up where a small minimum develops and successively disappears. This is not a cyclic-induced effect as a comparable behavior is observed for calendric aging (submitted soon). This was found in [10] to be caused by the anode overhang that induces an inhomogeneous SOC distribution at the edges of the active anode. Combined with the flat voltage curve in stage 1+2 of the graphite [30], this leads to a very slow compensation velocity of different SOCs on the anode.

Capacity loss of the anode active material is not noticeable, since the distance in x-direction between the characteristic peaks of the anode is not decreasing. Moreover, loss of cathode material is not observable as this would lead to a slope change increasing from 20 Ah on. Thus, it is concluded that the main aging mechanism for both cell types is loss of active lithium.

346 The observation that the shape of the DVA remains constant is a completely different result
347 compared to reported findings for shallow cycling for compressed cells [10] and cells with
348 limited space (cylindrical) [20] with as well NMC(1:1:1) and graphite electrodes. In [10] it
349 was discussed that cycling of compressed cells leads to a further broadening of the SOC
350 distribution and with this a lowering of HLD. As no such effect is observed in the here
351 presented test results, the impact of the presence of and absence of compression on a cells on
352 SOC distribution needs to show different results.

353 In an uncompressed cell, the compression is not counteracting the compensation currents
354 caused by different SOCs within the electrodes. Thus, the inhomogeneities in distribution of
355 active lithium caused during cycling is faster homogenized compared to a compressed cell,
356 shown in [22]. Inhomogeneities caused by anode overhang effect is especially observable in
357 [22] during and after cyclic aging and in [3] during calendric aging tests for average SOCs
358 that are already in the last plateau of the graphite anode. Combining Figure 6 and Figure 11
359 one can deduce that it takes 90 d at 20°C to recover peak shape, while in [3] it takes 250 d at
360 50°C in a calendric aging test. As the compensation velocity between electrode parts increases
361 besides voltage difference with increasing temperature, this is a clear evidence for faster
362 compensation in uncompressed cells. Furthermore, in [22] the homogenization was measured
363 for a compressed cell at 20°C after cycling. However, in that case the DVA shape hardly
364 changed over 200 d keeping the same storage potential. Only changing to SOC with a higher
365 slope on the anode speeds-up this process.

366 A more detailed view on HLD is obtained by evaluating the peak height at stage 2 (For
367 GEN-1 at 35 Ah in Figure 10 and for GEN-2 at 30 Ah in Figure 11) [10],[13],[22]. The
368 behavior of the GEN-1 cells is given in Figure 12a. A systematic error seems to have occurred
369 on the last two check-ups as the second last data point is very high and is not following the
370 overall trend. Unfortunately, the author have no answer to the origin of this error.

The peak heights for the GEN-2 are presented in Figure 12b. They deviate from the trends of the GEN-1 cell design in Figure 12a) on the first view. For both cell types, each curve of peak heights is associated to the corresponding full cell test SOC. However, associating the SOC related to the anode electrode (Table 2 right), the SOC values are shifted to each other and can be regrouped. According to their anode lithiation, the aging conditions are grouped by roman numbers from I to IV. I are SOCs lower than the first characteristic minimum of the graphite; II are SOCs between characteristic minima of the anode; III are SOCs directly at the minimum of the graphite at high SOC (stage 2); IV are SOCs on the last voltage plateau beyond stage 2. Grouping according to the graphite lithiation, the trends fit better to each other. As the anode-related SOC of GEN-1 is always lower than stage 2, the different behavior of the GEN-2 cell design at 68% and 80% SOC is not observed for GEN-1. Consequently, the peak height is depending mainly on the anode lithiation and not on the full cell SOC.

The anode for the GEN-2 cell is utilized to a higher degree (n/p ratio). Therefore, lithiation until stage 2 and beyond are measured only for GEN-2 cells (Figure 12b). At 80% SOC, the peak height initially reduces and increases smoothly thereafter. The test around 68% SOC has an extraordinary trend, as it is not decreasing but rising. At 45% SOC, the peak height remains constant for 300-400 cycles and increases thereafter. In [3],[10] it was claimed that the beginning of the constant increase in the last phase at around 300-500 FCE is an indicator for the end of the anode overhang effect with minimal contributions. This is in accordance to the trends found for capacity trend in the previous section.

A similar trend is observed for calendrically aged, compressed cell with comparable active materials [3]. Only the behavior at around 68% SOC is less dominant for the unconstrained pouch cell. The extraordinary behavior was correlated to the pressure gradient change and the voltage change at the same time [3]. However, the effect in an uncompressed cell is expected to be significantly weaker as compression of the stack is expected to have more impact as dilation of only the graphite anode.

4.4 Irreversible Aging

In the previous sections, the reversible effects on extractable capacity are discussed in-depth with respect to compression. In the following, the irreversible aging excluding reversible effects are presented and compared to compressed cells.

The reversible impact of the anode overhang on extractable capacity becomes negligible (after ca. 500 FCE) [3]. In the first order, the slope of the following near-linear part represents the aging rate of the cell type [22]. The influence on the slope by HLD is considered low as the peak height only for GEN-2, cycled around 80% SOC, is slightly lower than the initial one. For all other cells, the peak height is increased compared to the beginning. Kato et al. [26] showed that the increasing peak height above the initial value at about 50% SOC is not caused by further homogeneity increasing the amount of extractable capacity. They propose that instead the sharpening is not observable during charge and therefore this considered as no real gain in homogeneity. Thus, the impact on extractable capacity is regarded to be small. A good explanation for this phenomenon is obtained considering the previous charge period. In the last plateau after passing by stage 2, there is hardly any voltage difference (<1mV) that can compensate the inhomogeneities in the lithium distribution occurring in the charge phase. Assuming slippage of anode and cathode caused by only loss of active lithium, the time the cell is charged beyond stage 2 decreases. With this, the duration of dephasing the lithium distribution during charging reduces. In that case, the peak height is increasing with slippage and slippage is increasing with loss of active lithium. This is assumed the main reason for increasing peak height over aging during discharge. During charge no such change in peak height occurs as the voltage slope of graphite at the end of discharge is high. Only the anomalous increase of peak height measured for cell kept at stage 2 [3] is not satisfactorily explainable with this theory, so far.

The slopes to the aging rates from 500 FCE on are given in Figure 13. The shape of the trends reminds of an e-function and the aging rates reach their maximum at highest SOC. This is comparable to results reported for calendric aging tests for compressed prismatic cells [3], where the DVA shape is mainly preserved. In other publications like [20],[27],[28],[38], comparable results are reported. However, as the influence of the anode overhang effect is not considered, an explicit proof is hardly possible.

The results deviate significantly from the previously discussed compressed prismatic cells where the shape of the aging trend is more or less a u-shape and increases for higher and lower SOCs while the DVA strongly flattens [10]. The flattening of the DVA, and with this, the lower HLD decreases the extractable capacity leading to the u-shape. However, the low HLD is reversible and after relaxation, a comparable trend as for the uncompressed pouch cells appears [22]. The u-shape has been observed as well for a cylindrical cell by Ecker et al [20],[34]. Consequently, the uncompressed cells seem to be less affected by increasing inhomogeneities compared to compressed cells. Certainly, increasing currents and decreasing temperature will lead for all cell types and compressions to inhomogeneities and lithium plating [6],[16]. However, at moderate cyclic aging conditions, the HLD is hardly changing. In [6],[34] it is reported that for pouch cells lithium metal deposition takes place close to the edge of the sheets where the aluminum pouch foil is welded. This matches to the theory, as the expansion during cycling is limited towards the edges making this area more prone to lithium metal deposition. However, the uncompressed cells might accept less current density compared to a compressed cell. This means that in case lithium plating occurs, it takes place on a larger area simultaneously.

Comparing the GEN-1 and the GEN-2 cell design the aging for GEN-1 is lower. This is assumed to be caused by the higher n/p ratio of the GEN-1 compared to the GEN-2 leading to a lower current density on the anode and a lower local risk of lithium metal deposition.

Furthermore, the proposed admixture of hard carbons to the anode of the GEN-1 cell design increases the power capability of the electrode and decreases as well the risk of lithium metal deposition. A smaller anode overhang is not considered to reduce lifetime. In contrast, the smaller anode overhang reduces the amount of active lithium lost in SEI especially during formation (not considered here).

In order to understand the optimization strategy between the two generations, the FCE are estimated for the arbitrary end-of-life criterion of 80% SOH in Figure 14. For that case, the cycle time for the corresponding cell has been calculated. Both cell designs reach at 20°C cycle lives of more than 7,799 FCE and minimum 2.6 years equivalent test time (ETT). For every test condition, GEN-1 is always above and GEN-2 always below 20,000 FCE. Supposing one full cycle per day, 20,000 FCE correspond to a lifetime of roughly 55 years. This is far beyond the targeted lifetime in automotive industries of 10-20 years. Therefore, it seems that it was the strategy of the company Litarion to manufacture cells with lower cycle life to increase energy density and reduce potentially costs, as the cyclic stability is not necessary for many applications.

Conclusions

In this paper, 24 uncompressed pouch bag cells are investigated during 6% DOD cycle tests at five different test SOCs. They are subdivided in a GEN-1 and a GEN-2 cell design. The GEN-2 has a lower amount of anode overhang, a lower n/p ratio and a higher energy density. For both cell designs, it was shown that compressed cells have a very different behavior compared to uncompressed pouch cells. While shallow cycling of compressed cells accumulates inhomogeneities, the cycling induced inhomogeneities in uncompressed pouch cells are not measurable under comparable test conditions. The homogeneity of lithium distribution (HLD) is measured by evaluation of DVA characteristics. The results in DVA shape, and with this, in HLD are comparable to calendric aging tests independent of the external compression. As the two examined cell designs have a different n/p ratio, it was shown that the peak heights dependent mainly on the degree of anode lithiation.

The contribution of the anode overhang is lower than expected and only the near part is usable in a reasonable time. As the capacity difference over aging is not declining, it is assumed that near parts of the anode overhang are actively charge- and dischargeable within a 0.1C cycle. For compressed cells, the capacity difference reduces in the same way for all cell designs. Therefore, it was concluded that for compressed cells the lithium-ion movement at the interface anode overhang-active anode becomes slower over aging until finally no significant contribution over one cycle takes place.

The irreversible capacity loss, measured by the linear slope of the last part of capacity trend, is clearly lower for the GEN-1 cell design. On one side, this was attributed to the positive influence of the higher n/p ratio and on the other side to the admixture of hard carbons in the anode for the GEN-1 cell design. For both cell designs, the aging increases with SOC or cell voltage. Only at very low SOCs, higher aging rates are measured.

Acknowledgement

The results are generated during the project *Anode aging / Anodenalterung* (IGF 18779 N) with support of Litarion. We like to thank the Federal Ministry of Economics and Technology (Bundesministerium für Wirtschaft und Technologie - BMWi) for funding. Special thanks to the support by Frank Meier, Rita Graff, Lidiya Komsyiska and Pouyan Shafiei Sabet.

References

[1] J.P. Singer, T. Kropp, M. Kuehnemund, K.P. Birke, J. Electrochem. Soc. 165 (2018) A1348-A1356. https://doi.org/10.1149/2.0501807jes.

[2] J. Christensen, J. Newman, J Solid State Electrochem 10 (2006) 293–319. https://doi.org/10.1007/s10008-006-0095-1.

[3] M. Lewerenz, G. Fuchs, L. Becker, D.U. Sauer, Journal of Energy Storage 18 (2018) 149–159. https://doi.org/10.1016/j.est.2018.04.029.

[4] M. Hahn, H. Buqa, P.W. Ruch, D. Goers, M.E. Spahr, J. Ufheil, P. Novák, R. Kötz, Electrochem. Solid-State Lett. 11 (2008) A151. https://doi.org/10.1149/1.2940573.

[5] F. Grimsmann, F. Brauchle, T. Gerbert, A. Gruhle, J. Parisi, M. Knipper, Journal of Energy Storage 14 (2017) 158–162. https://doi.org/10.1016/j.est.2017.10.010.

[6] J. Sturm, F.B. Spingler, B. Rieger, A. Rheinfeld, A. Jossen, J. Electrochem. Soc. 164 (2017) A1342-A1351. https://doi.org/10.1149/2.0161707jes.

[7] D.J. Xiong, L.D. Ellis, K.J. Nelson, T. Hynes, R. Petibon, J.R. Dahn, J. Electrochem. Soc. 163 (2016) A3069-A3077. https://doi.org/10.1149/2.1031614jes.

[8] M. Wünsch, J. Kaufman, D.U. Sauer, Journal of Energy Storage 21 (2019) 149–155. https://doi.org/10.1016/j.est.2018.11.019.

[9] M. Lewerenz, A. Warnecke, D.U. Sauer, Journal of Power Sources 369 (2017) 122–132. https://doi.org/10.1016/j.jpowsour.2017.10.003.

[10] M. Lewerenz, D.U. Sauer, Journal of Energy Storage 18 (2018) 421–434. https://doi.org/10.1016/j.est.2018.06.003.

[11] A.S. Mussa, M. Klett, G. Lindbergh, R.W. Lindström, Journal of Power Sources 385 (2018) 18–26. https://doi.org/10.1016/j.jpowsour.2018.03.020.

[12] J. Cannarella, C.B. Arnold, Journal of Power Sources 245 (2014) 745–751. https://doi.org/10.1016/j.jpowsour.2013.06.165.

[13] M. Lewerenz, A. Marongiu, A. Warnecke, D.U. Sauer, Journal of Power Sources 368 (2017) 57–67. https://doi.org/10.1016/j.jpowsour.2017.09.059.

[14] T.C. Bach, S.F. Schuster, E. Fleder, J. Müller, M.J. Brand, H. Lorrmann, A. Jossen, G. Sextl, Journal of Energy Storage 5 (2016) 212–223. https://doi.org/10.1016/j.est.2016.01.003.

[15] M.H. Hofmann, K. Czyrka, M.J. Brand, M. Steinhardt, A. Noel, F.B. Spingler, A. Jossen, Journal of Energy Storage 20 (2018) 120–133. https://doi.org/10.1016/j.est.2018.08.013.

[16] F.B. Spingler, W. Wittmann, J. Sturm, B. Rieger, A. Jossen, Journal of Power Sources 393 (2018) 152–160. https://doi.org/10.1016/j.jpowsour.2018.04.095.

[17] C.-W. Wang, Y.-B. Yi, A.M. Sastry, J. Shim, K.A. Striebel, J. Electrochem. Soc. 151 (2004) A1489. https://doi.org/10.1149/1.1783909.
[18] C. Meyer, H. Bockholt, W. Haselrieder, A. Kwade, Journal of Materials Processing Technology 249 (2017) 172–178. https://doi.org/10.1016/j.jmatprotec.2017.05.031.
[19] J. Cannarella, C.B. Arnold, Journal of the Electrochemical Society (2015) A1365-A1373.
[20] M. Ecker, N. Nieto, S. Käbitz, J. Schmalstieg, H. Blanke, A. Warnecke, D.U. Sauer, Journal of Power Sources 248 (2014) 839–851. https://doi.org/10.1016/j.jpowsour.2013.09.143.
[21] E. Sarasketa-Zabala, I. Gandiaga, E. Martinez-Laserna, L.M. Rodriguez-Martinez, I. Villarreal, Journal of Power Sources 275 (2015) 573–587. https://doi.org/10.1016/j.jpowsour.2014.10.153.
[22] M. Lewerenz, P. Dechent, D.U. Sauer, Journal of Energy Storage 21 (2019) 680–690. https://doi.org/10.1016/j.est.2019.01.004.
[23] B. Epding, B. Rumberg, H. Jahnke, I. Stradtmann, A. Kwade, Journal of Energy Storage 22 (2019) 249–256. https://doi.org/10.1016/j.est.2019.02.015.
[24] T.R.B. Grandjean, J. Groenewald, A. McGordon, J. Marco, Journal of Energy Storage 24 (2019) 100804. https://doi.org/10.1016/j.est.2019.100804.
[25] E. Sarasketa-Zabala, I. Gandiaga, L.M. Rodriguez-Martinez, I. Villarreal, Journal of Power Sources 272 (2014) 45–57. https://doi.org/10.1016/j.jpowsour.2014.08.051.
[26] H. Kato, Y. Kobayashi, H. Miyashiro, Journal of Power Sources 398 (2018) 49–54. https://doi.org/10.1016/j.jpowsour.2018.07.043.
[27] S. Käbitz, J.B. Gerschler, M. Ecker, Y. Yurdagel, B. Emmermacher, D. André, T. Mitsch, D.U. Sauer, Journal of Power Sources 239 (2013) 572–583. https://doi.org/10.1016/j.jpowsour.2013.03.045.
[28] P. Keil, S.F. Schuter, J. Wilhelm, J. Travi, A. Hauser, R.C. Katl, A. Jossen, Journal of the Electrochemical Society (2016) A1872-A1880. https://doi.org/10.1149/2.0411609jes.
[29] M. Wilamowska, M. Graczyk-Zajac, R. Riedel, Journal of Power Sources 244 (2013) 80–86. https://doi.org/10.1016/j.jpowsour.2013.03.137.
[30] J.R. Dahn, Physical Review B (1991) 9170–9177. https://doi.org/10.1103/PhysRevB.44.9170.
[31] M. Lewerenz, J. Münnix, J. Schmalstieg, S. Käbitz, M. Knips, D.U. Sauer, Journal of Power Sources 345 (2017) 254–263. https://doi.org/10.1016/j.jpowsour.2017.01.133.
[32] T. Dagger, J. Kasnatscheew, B. Vortmann-Westhoven, T. Schwieters, S. Nowak, M. Winter, F.M. Schappacher, Journal of Power Sources 396 (2018) 519–526. https://doi.org/10.1016/j.jpowsour.2018.06.043.
[33] B. Gyenes, D.A. Stevens, V.L. Chevrier, J.R. Dahn, Journal of the Electrochemical Society 162 (2015) A278-A283. https://doi.org/10.1149/2.0191503jes.
[34] Alexander Johannes Warnecke, Dissertation, RWTH Aachen University (2017). https://doi.org/10.18154/RWTH-2017-09646.
[35] V. Agubra, J. Fergus, Materials (Basel, Switzerland) 6 (2013) 1310–1325. https://doi.org/10.3390/ma6041310.
[36] A.J. Smith, Dahn Hannah M., J.C. Burns, J.R. Dahn, Journal of the Electrochemical Society (2012) A705-A710. https://doi.org/10.1149/2.056206jes.
[37] M. Lewerenz, A. Warnecke, D.U. Sauer, Journal of Power Sources 354 (2017) 157–166. https://doi.org/10.1016/j.jpowsour.2017.04.043.
[38] D. Li, D.L. Danilov, J. Xie, L. Raijmakers, L. Gao, Y. Yang, P.H.L. Notten, Electrochimica Acta 190 (2016) 1124–1133. https://doi.org/10.1016/j.electacta.2015.12.161.

Annex

The n/p ratio is defined as follows: It cannot be simply calculated as the cathode is only partly delithiated. Thus, the usable capacity after formation is defined as cathode capacity $C_{cathode}$ (although even more capacity can be charged and discharged). The anode capacity C_{anode} is defined by peak at stage 2 (MinHi) multiplied with 2 as this is the point where graphite is lithiated by 50% [30].

$$C_{anode}/C_{cathode} = \frac{(C_{Nom} - MinHi) \cdot 2}{C_{Nom}} \quad (2)$$

The n/p ratio is only defined to give the reader a fast impression of the overdimensioning of the anode compared to the cathode for the GEN-1 and the GEN-2 cell design.

Figure Captions:

Figure 1 **Average SOCs at the begin of test depicted in a) the 0.1C discharge curve, b) the corresponding DVA and c) the corresponding potentials of graphite vs. lithium metal half-cell measurement correlated to the full cell via DVA. The homogeneity will be measured according to the height evolution during aging of MinHi at stage 2 of the graphite according to b).**

Figure 2 **Comparison of geometrical areas of the anode and the cathode for a) GEN-1 and b) GEN-2. The anode overhang and the stacking is shown generally in c).**

Figure 3 **Lasermicroscope images of the pristine a) anode and c) cathode of the GEN-1 and the b) anode and d) cathode of the GEN-2 cell design.**

Figure 4 **Voltage characteristics of the half-cell (HC) curves (solid line) and their derivatives (dashed line). In a) is the anode and in b) the cathode of the GEN-1 (blue) and the GEN-2 (red) cell design.**

Figure 5 Displacement measurement during a 0.1C discharge at two positions (solid and dashed line) for a) the GEN-1 (blue) and for the GEN-2 (red) cell design. Further, in b) the displacement is compared to the corresponding DVA.

Figure 6 Extractable capacity and internal resistance over FCE for a)+c) the GEN-1 and for b)+d) the GEN-2 cell design. The cells are aged at 1C and 6% DOD around specific average SOC. The capacity is measured at 0.1C.

Figure 7 Comparison of lithium-ion migration between the calculated near anode overhang and the results obtained from the linear extrapolation a) for the GEN-1 and b) for the GEN-2 cell design.

Figure 8: Lasermicroscope images of the overhang of a pristine, a GEN-1 and a GEN-2 cell of the first electrode sheet; outer and inner side

Figure 9 Capacity difference $C_{0.1C}$-C_{1C} for all five SOCs over aging for a) the GEN-1 and b) for the GEN-2 cell design. The grey bar represents the corridor that is reached in the end by all calendric aging tests.

Figure 10 Series of DVA for five SOC over aging for the GEN-1 cell design. The color-coding of the color bar links the extractable capacity to the corresponding DVA.

Figure 11 Series of DVA for five SOC over aging for the GEN-2 cell design. The color-coding of the color bar links the extractable capacity to the corresponding DVA.

Figure 12 Peak height of the minimum at high SOC for all five SOCs over aging for a) the GEN-1 and b) for the GEN-2 cell design. In roman numbers the SOC are grouped according to the graphite lithiation.

Figure 13 Slopes of the linear fitted part of capacity trend are plotted for all five SOCs over test SOC of the full cell for the GEN-1 and for the GEN-2 cell design.

Figure 14 Left axis: FCE until the SOH of 80% is reached. Right axis: the equivalent test time (ETT) until the SOH of 80% is reached.

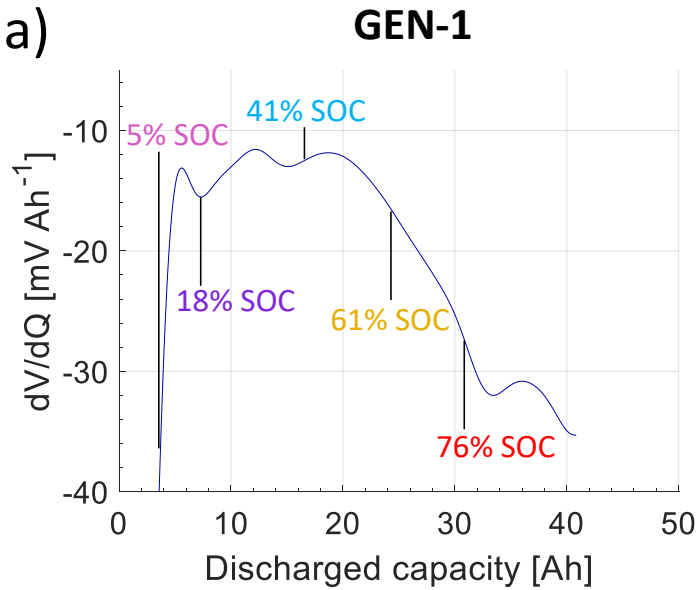
a)
GEN-1
5% SOC
41% SOC
18% SOC
61% SOC
76% SOC
dV/dQ [mV Ah-1]
-10
-20
-30
-40
0
10
20
30
40
50
Discharged capacity [Ah]

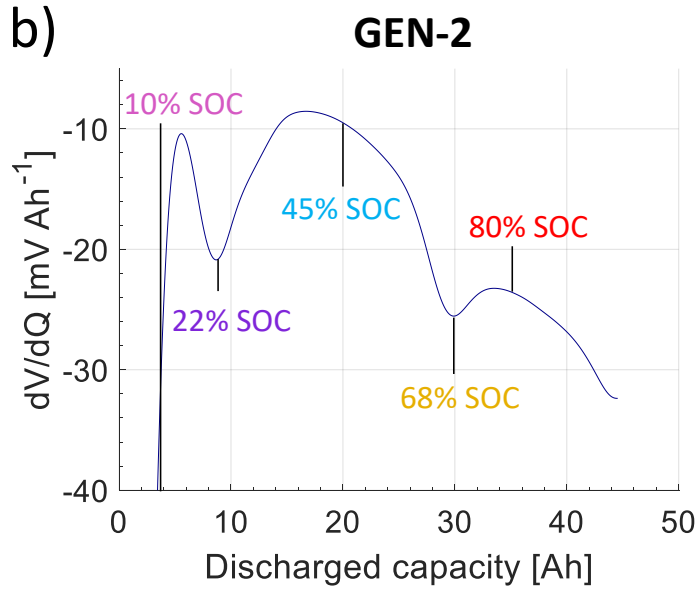
b)
GEN-2
10% SOC
45% SOC
80% SOC
22% SOC
68% SOC
dV/dQ [mV Ah-1]
-10
-20
-30
-40
0
10
20
30
40
50
Discharged capacity [Ah]

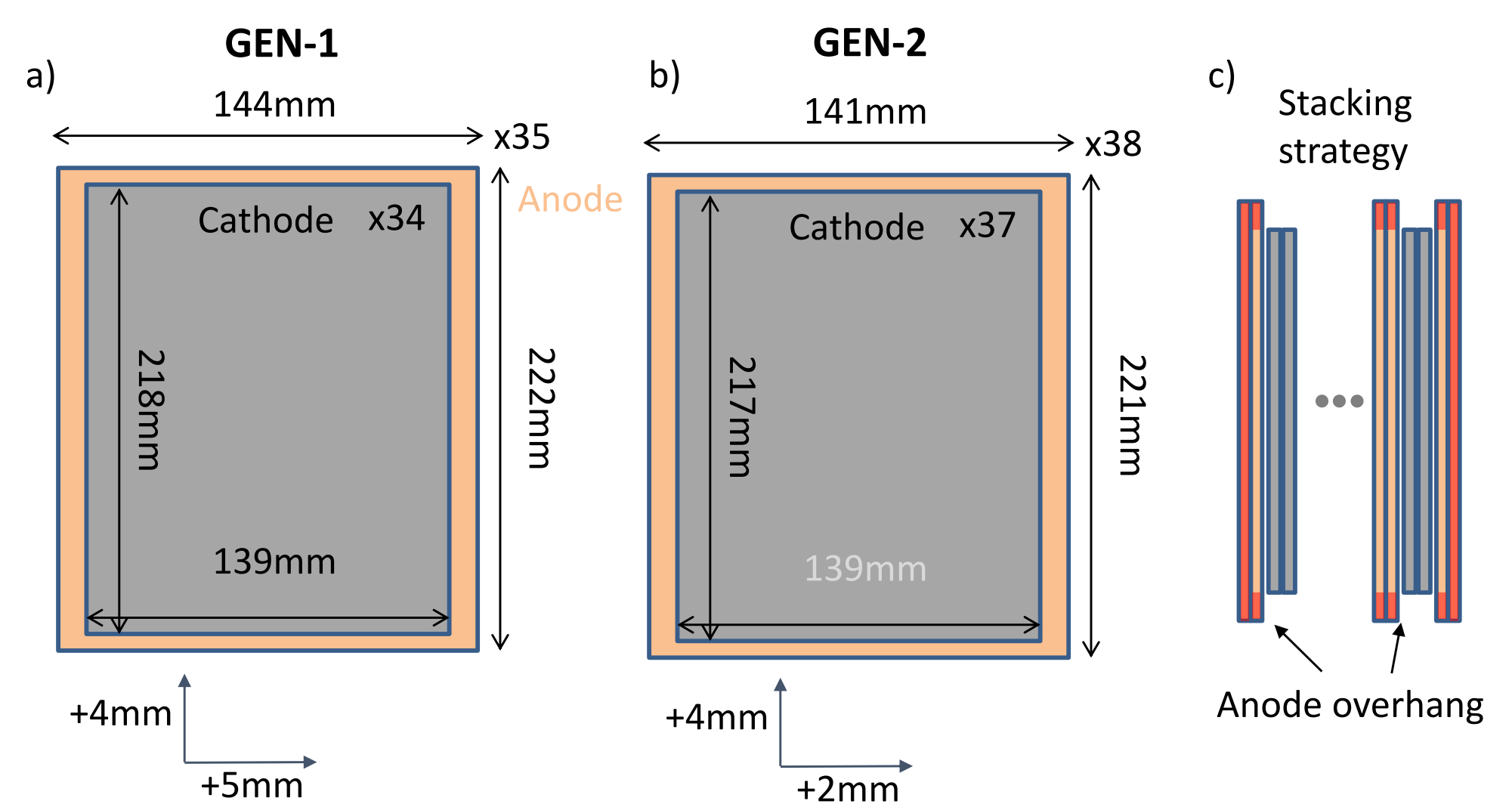
GEN-1
a)
144mm
x35
Anode
Cathode x34
218mm
222mm
139mm
+4mm
+5mm
GEN-2
b)
141mm
x38
Cathode x37
217mm
221mm
139mm
+4mm
+2mm
c)
Stacking strategy
Anode overhang

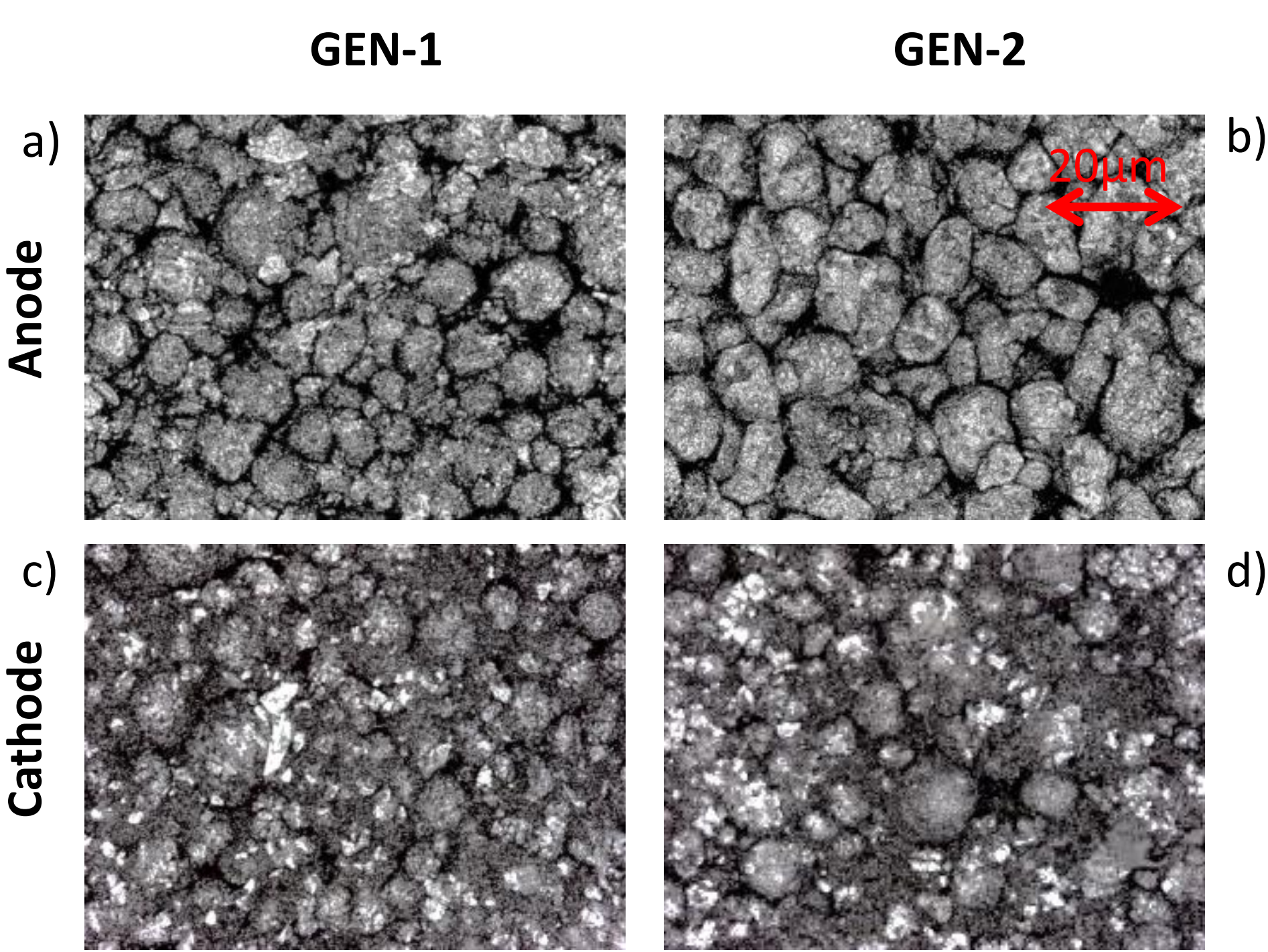
GEN-1
GEN-2
a)
b)
Anode
20µm
c)
d)
Cathode

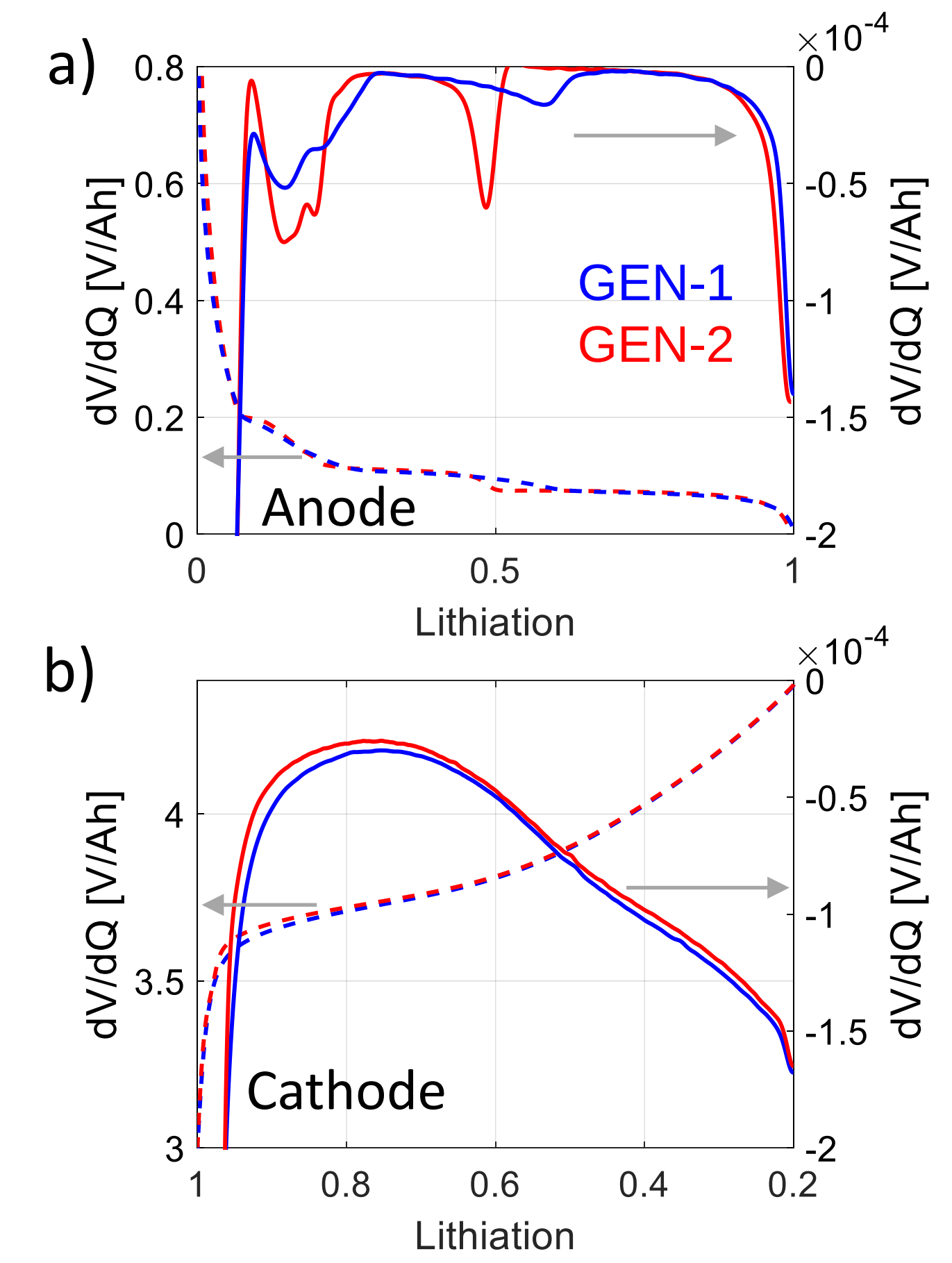
a)
0.8
0.6
0.4
0.2
0
dV/dQ [V/Ah]
×10-4
0
-0.5
-1
-1.5
-2
dV/dQ [V/Ah]
GEN-1
GEN-2
Anode
0
0.5
1
Lithiation
b)
4
3.5
3
dV/dQ [V/Ah]
×10-4
0
-0.5
-1
-1.5
-2
dV/dQ [V/Ah]
Cathode
1
0.8
0.6
0.4
0.2
Lithiation

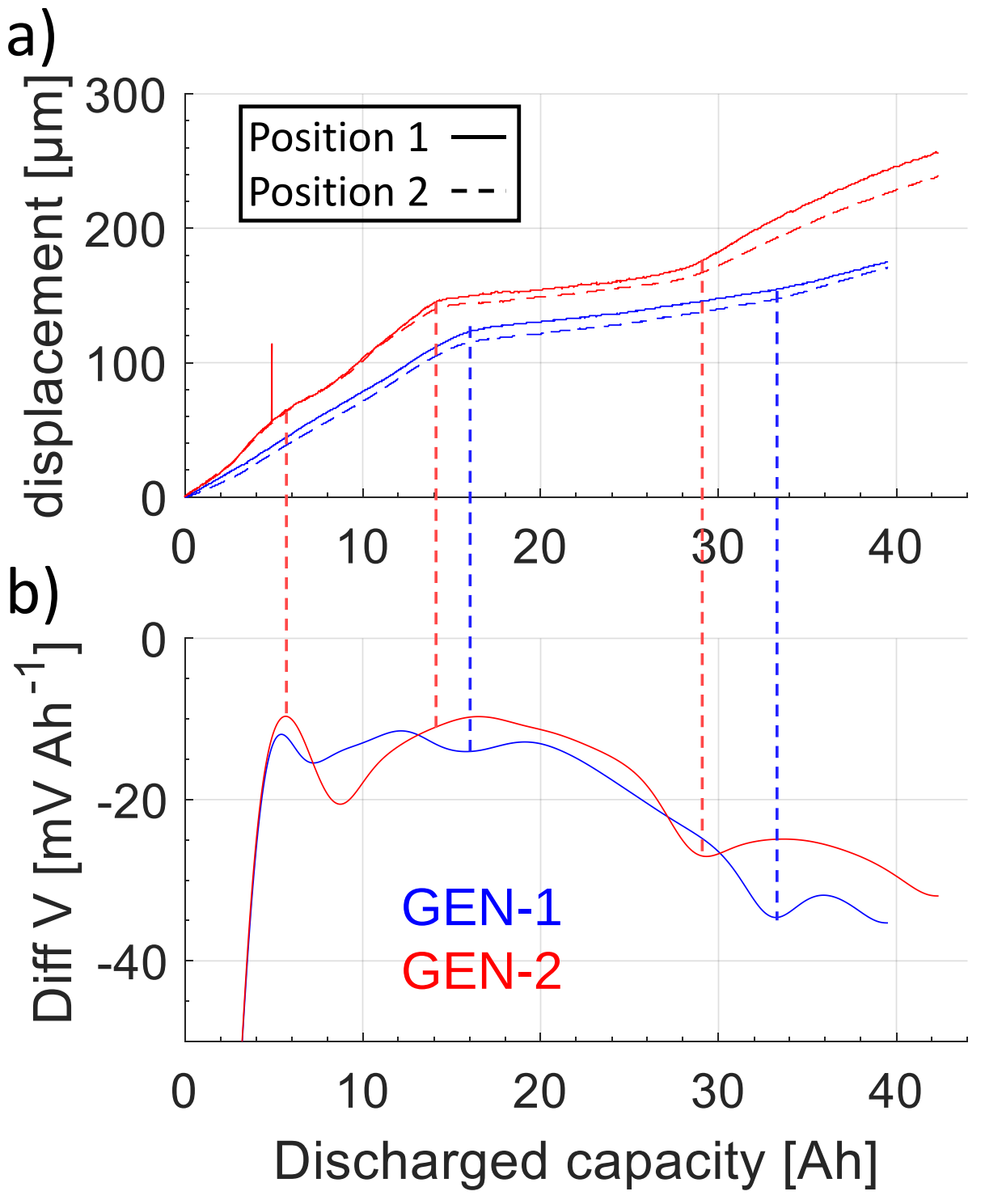
a)
displacement [µm]
300
200
100
0
Position 1
Position 2
0
10
20
30
40
b)
Diff V [mV Ah^{-1}]
0
-20
-40
GEN-1
GEN-2
0
10
20
30
40
Discharged capacity [Ah]

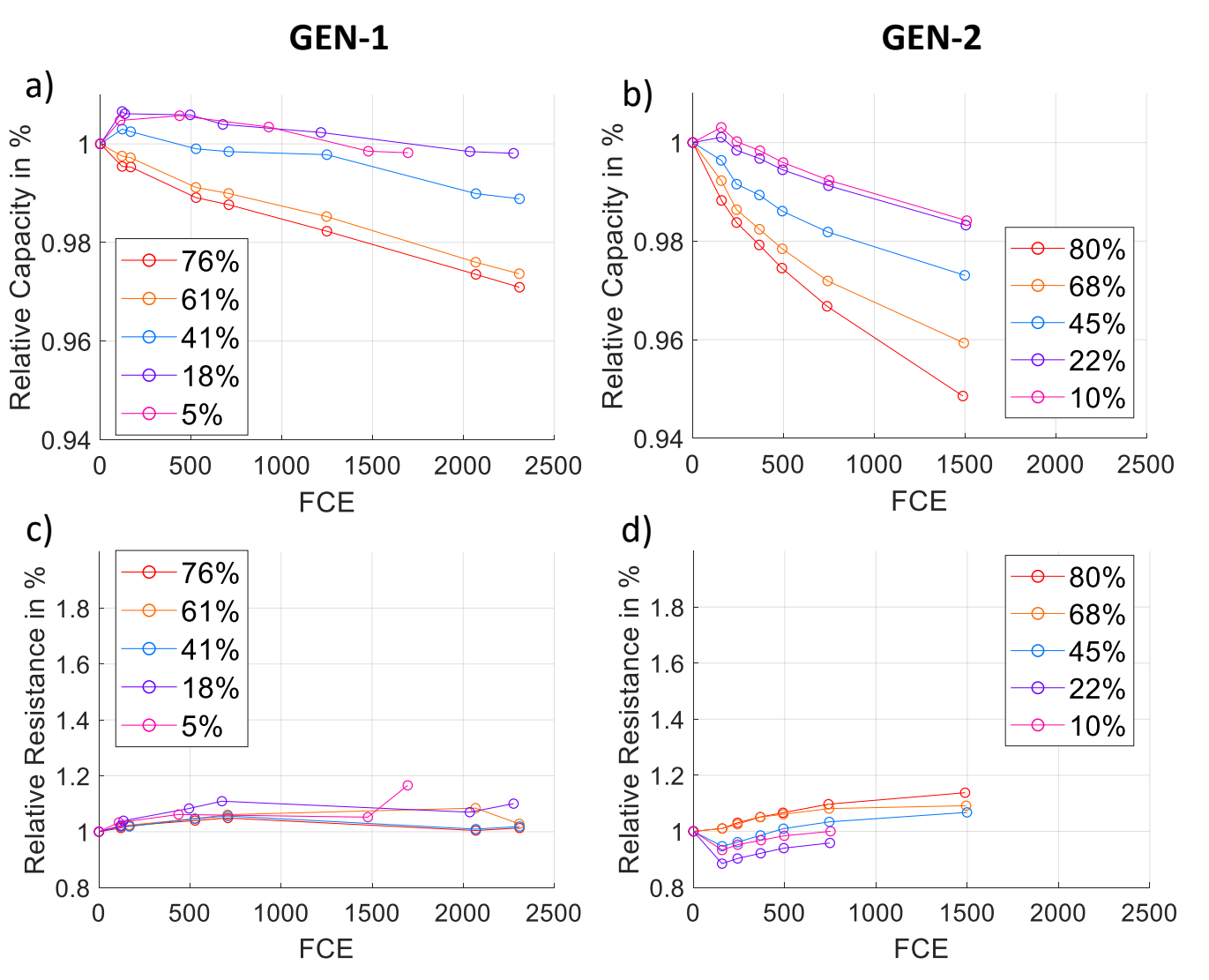
GEN-1
GEN-2
a)
b)
c)
d)
Relative Capacity in %
Relative Resistance in %
FCE
76%
61%
41%
18%
5%
80%
68%
45%
22%
10%
0.94
0.96
0.98
1
0.8
1.2
1.4
1.6
1.8
0
500
1000
1500
2000
2500

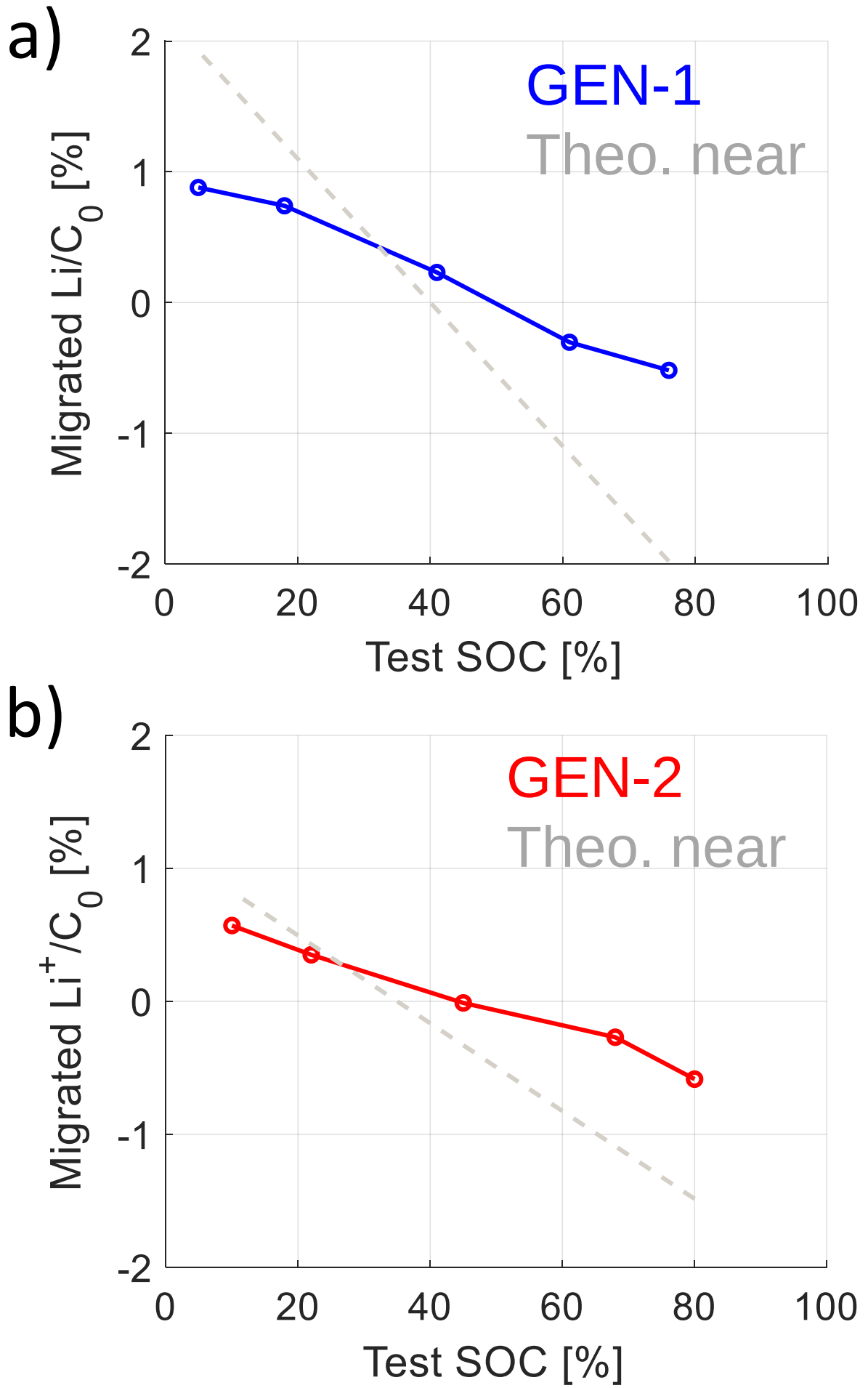
a)
GEN-1
Theo. near
Migrated Li/C0 [%]
Test SOC [%]
b)
GEN-2
Theo. near
Migrated Li+/C0 [%]
Test SOC [%]

	Picture outer anode	Overhang outer side	Overhang inner side
Pristine cell (GEN-1)	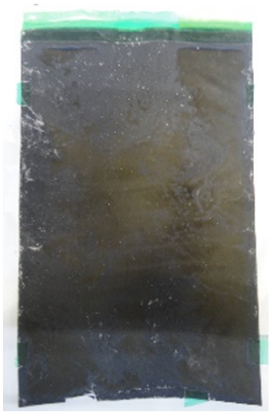	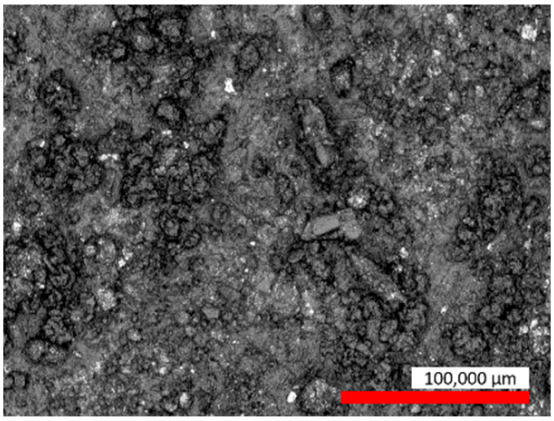	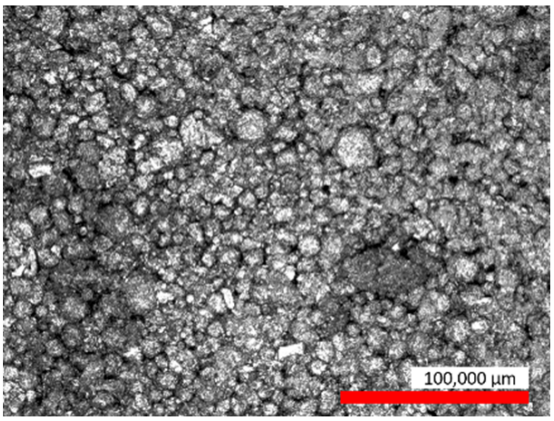
GEN-1 5% SoC, 6% DoD, 20°C		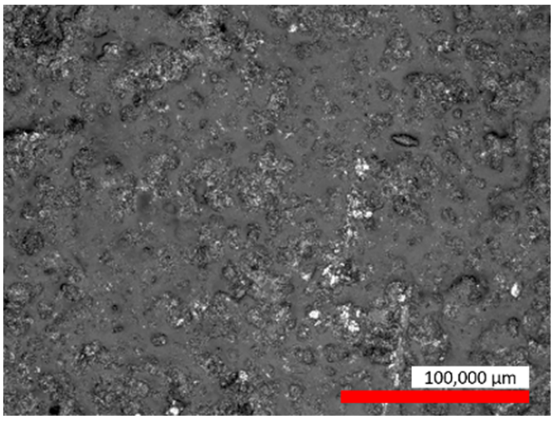	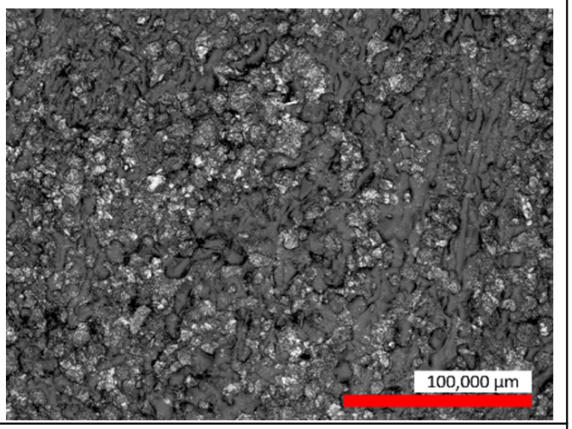
GEN-2 80% SoC, 6% DoD, 20°C	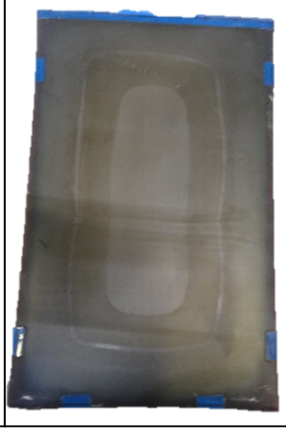	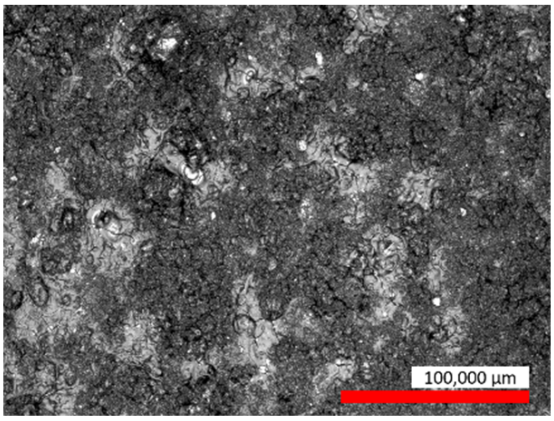	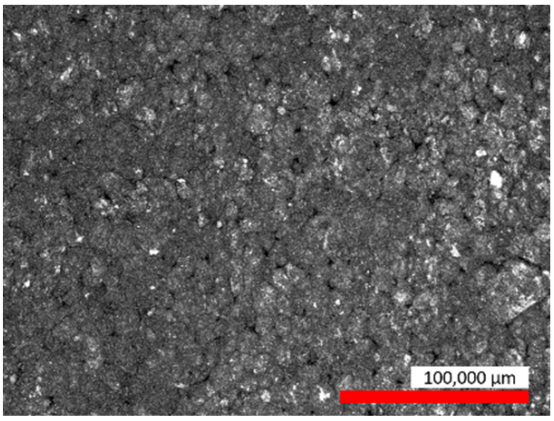

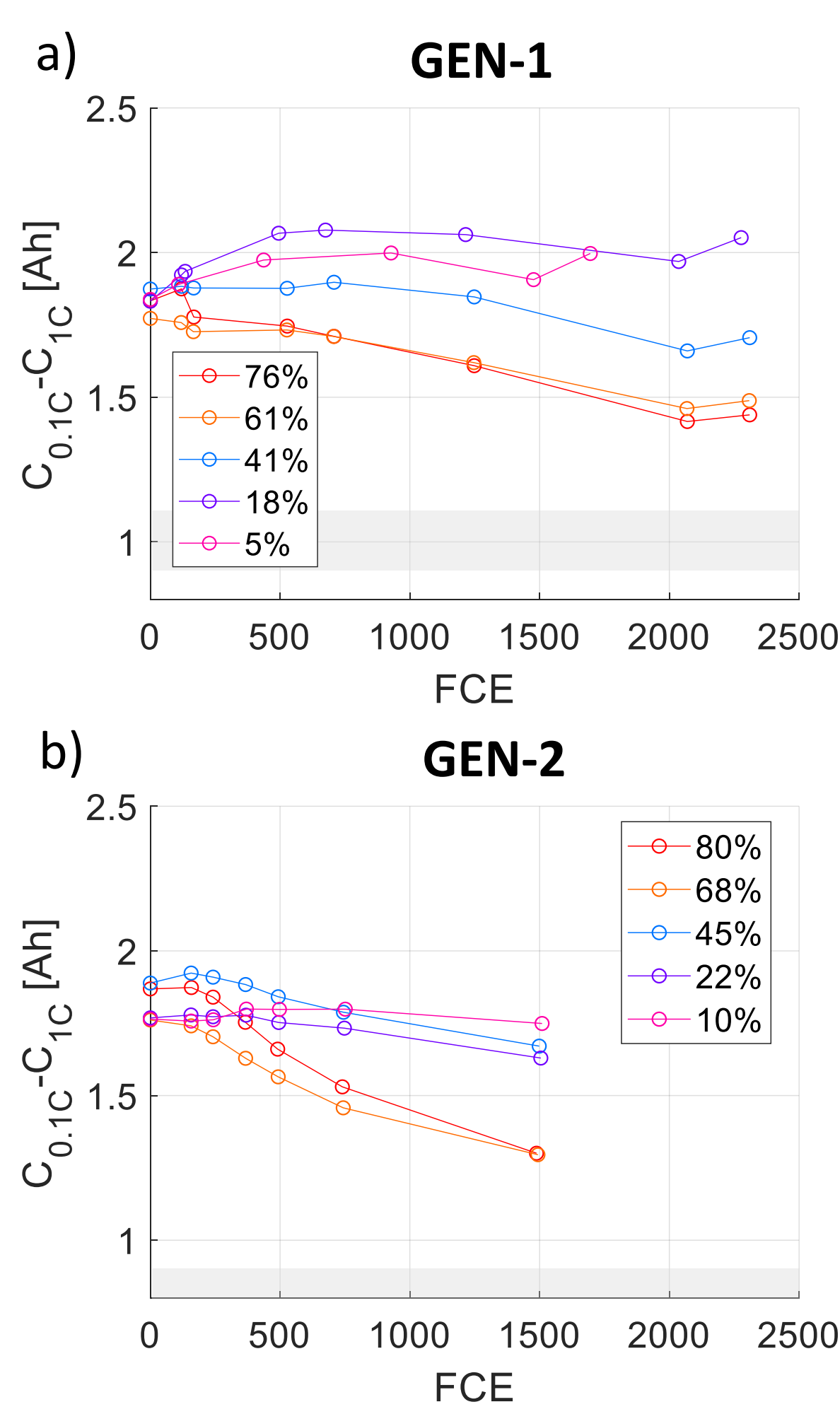
a)
GEN-1
2.5
2
1.5
1
$C_{0.1C}$-C_{1C} [Ah]
76%
61%
41%
18%
5%
0
500
1000
1500
2000
2500
FCE
b)
GEN-2
2.5
2
1.5
1
$C_{0.1C}$-C_{1C} [Ah]
80%
68%
45%
22%
10%
0
500
1000
1500
2000
2500
FCE

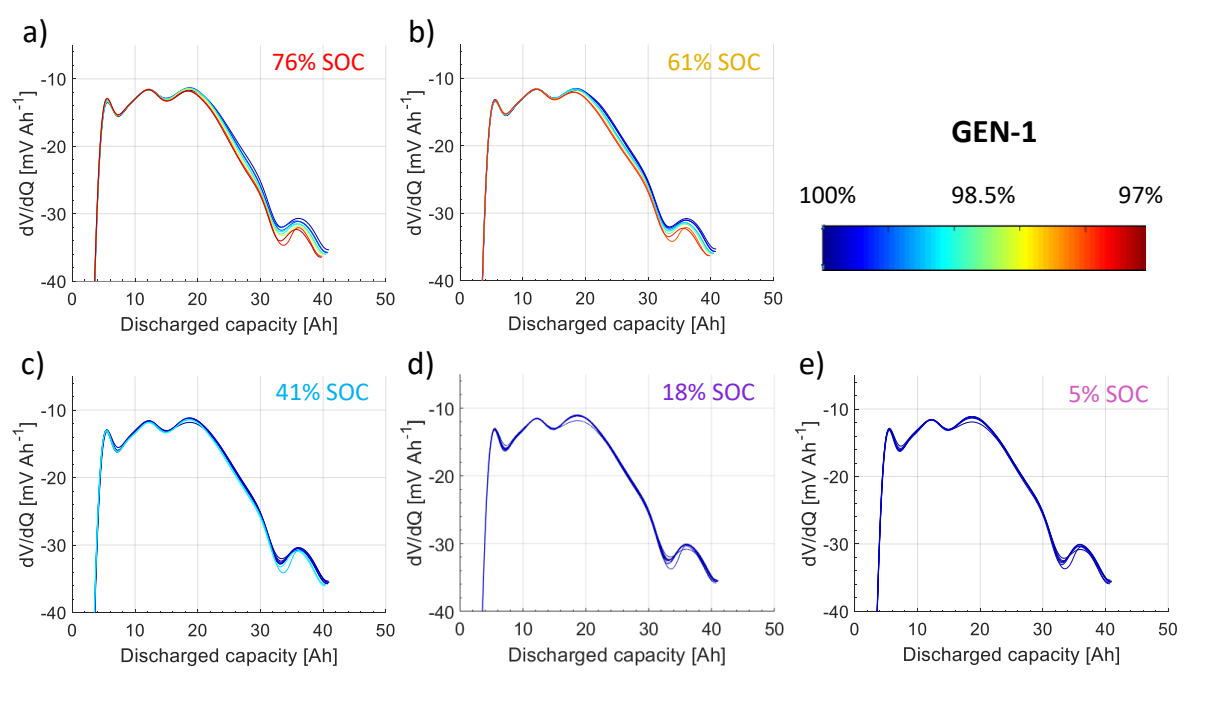
a)
76% SOC
b)
61% SOC
GEN-1
100%
98.5%
97%
c)
41% SOC
d)
18% SOC
e)
5% SOC
dV/dQ [mV Ah^{-1}]
Discharged capacity [Ah]

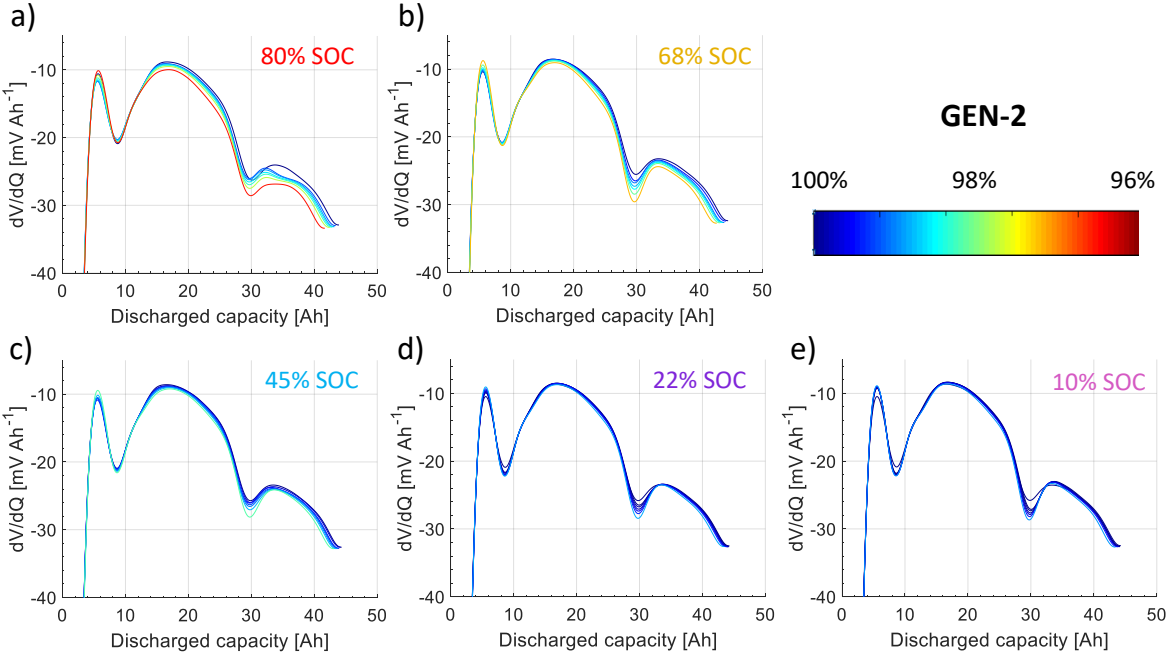
a)
80% SOC
b)
68% SOC
GEN-2
100%
98%
96%
c)
45% SOC
d)
22% SOC
e)
10% SOC
dV/dQ [mV Ah^{-1}]
Discharged capacity [Ah]

a)

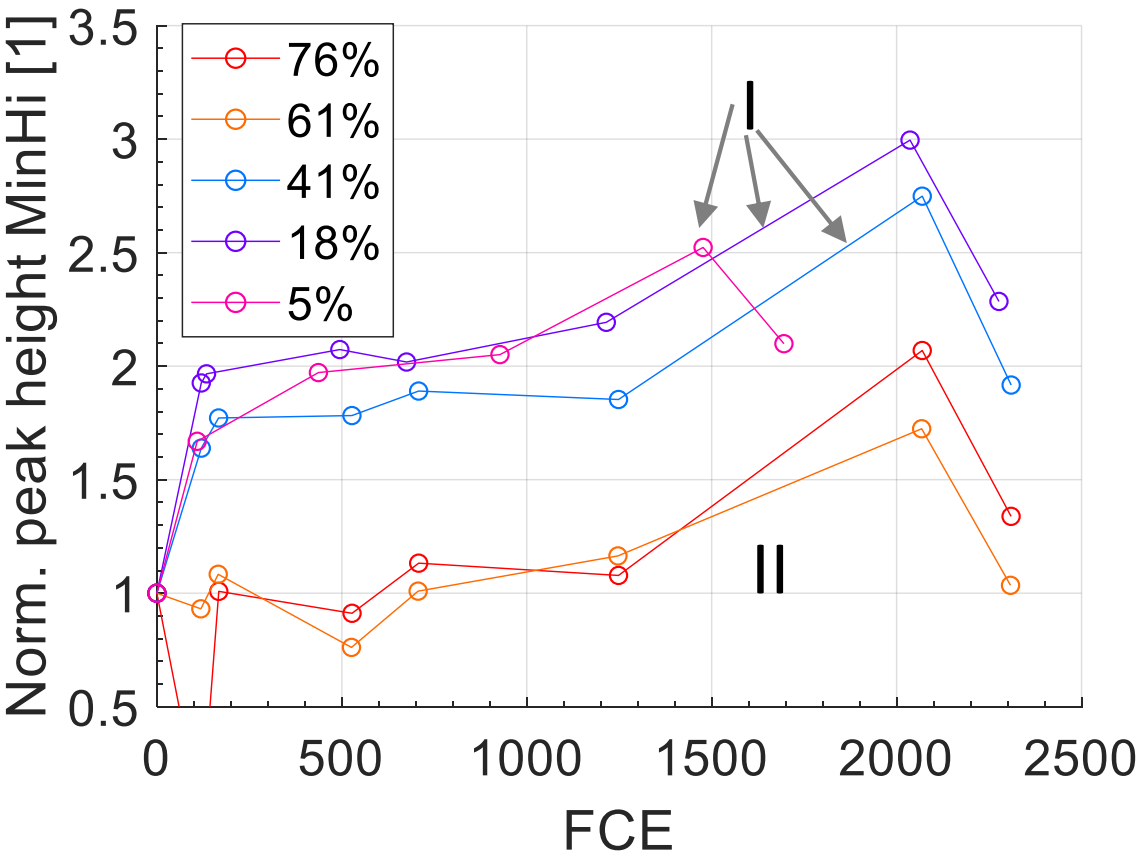
GEN-1
Norm. peak height MinHi [1]
3.5
3
2.5
2
1.5
1
0.5
0
500
1000
1500
2000
2500
FCE
76%
61%
41%
18%
5%
I
II

b)

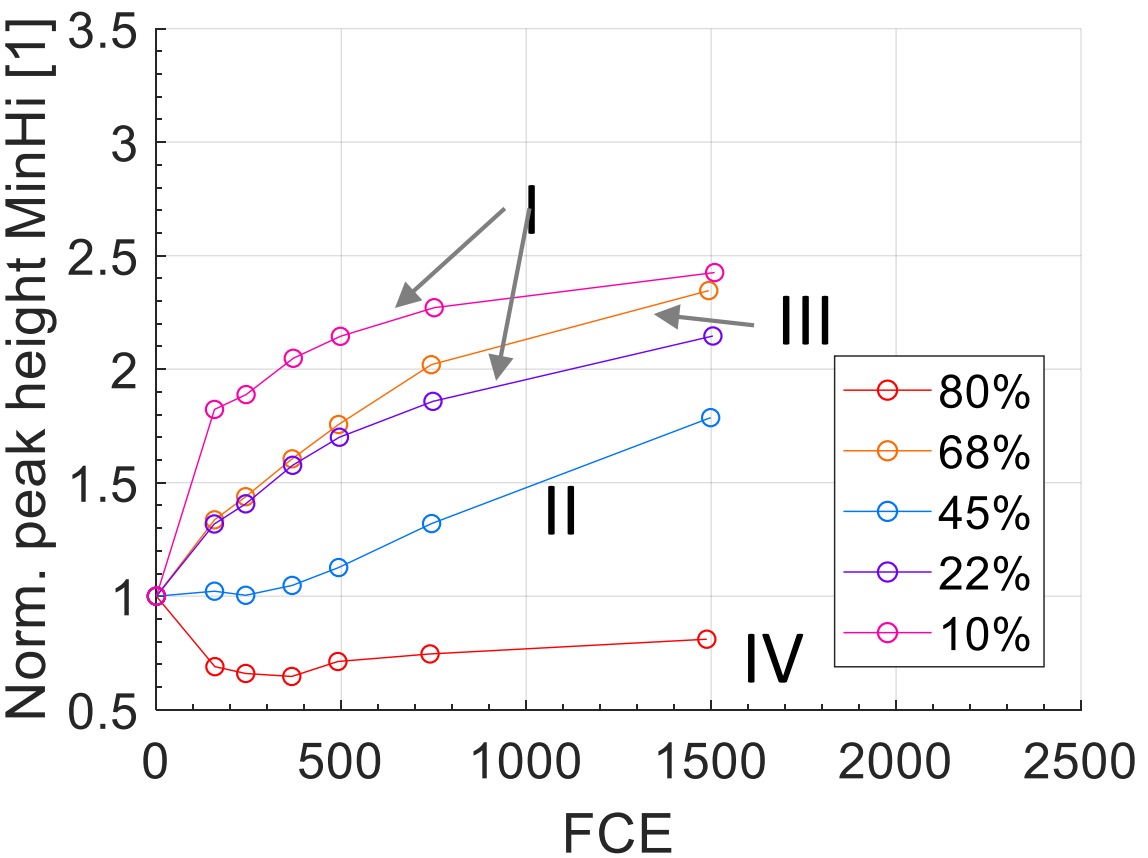
GEN-2
Norm. peak height MinHi [1]
3.5
3
2.5
2
1.5
1
0.5
0
500
1000
1500
2000
2500
FCE
80%
68%
45%
22%
10%
I
II
III
IV

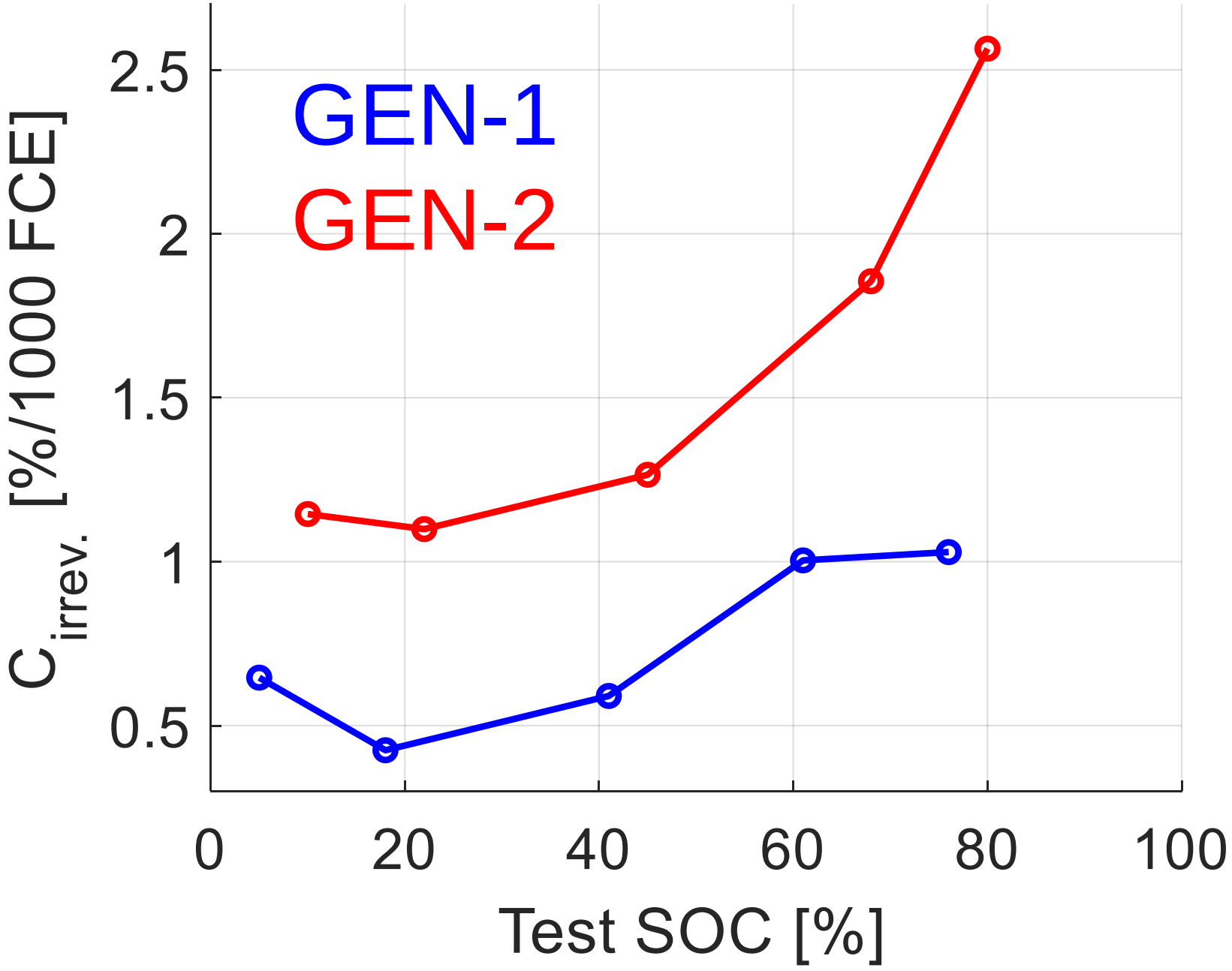
GEN-1
GEN-2
2.5
2
1.5
1
0.5
$C_{irrev.}$ [%/1000 FCE]
0
20
40
60
80
100
Test SOC [%]

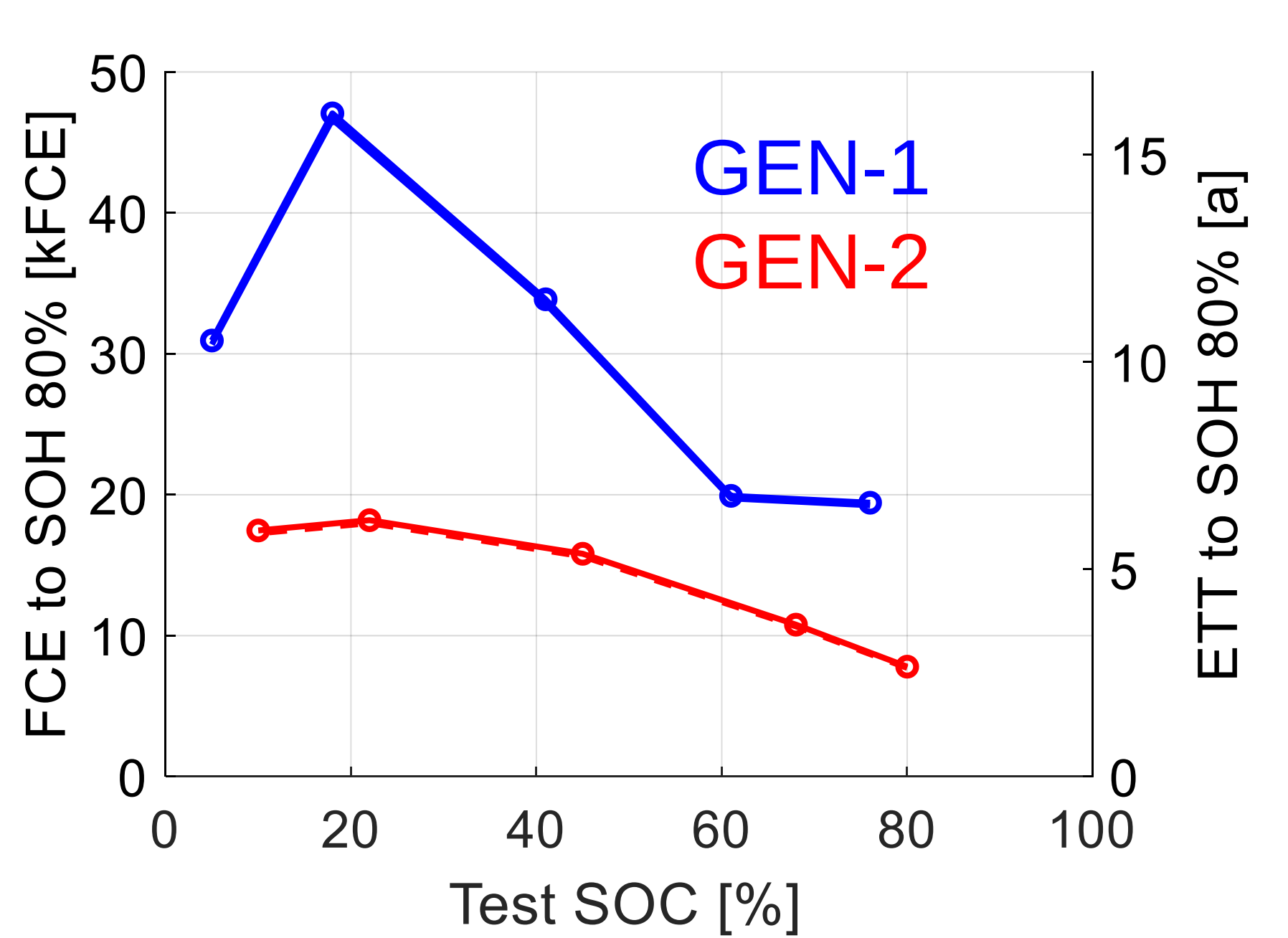
GEN-1
GEN-2
FCE to SOH 80% [kFCE]
ETT to SOH 80% [a]
Test SOC [%]
0
10
20
30
40
50
0
5
10
15
0
20
40
60
80
100